Sustainable Cities and Society 53 (2020) 101962

Contents lists available at ScienceDirect

Sustainable Cities and Society

journal homepage: www.elsevier.com/locate/scs

Developing a rapid method for 3-dimensional urban morphology extraction using open-source data

Chao Ren[a], Meng Cai[b,*], Xinwei Li[a], Yuan Shi[b], Linda See[c]

[a] Faculty of Architecture, The University of Hong Kong, Hong Kong, China
[b] School of Architecture, The Chinese University of Hong Kong, Shatin, N.T., Hong Kong, China
[c] International Institute for Applied Systems Analysis (IIASA), Laxenburg, Austria

ARTICLE INFO

Keywords:
Urban morphology extraction
Open-source data
Open map service
Morphological parameters
Satellite images

ABSTRACT

Available and accessible three-dimensional (3D) urban morphology data have become essential for extensive academic research on built-up environments and urban climates. A rapid and consistent methodology for extracting urban morphology information is urgently needed for sustainable urban development in global cities, particularly given future trends of rapid urbanization. However, there is still a lack of generally applicable methods that use open-source data in this context. In this study, we developed a simple and highly efficient method for acquiring 3D urban morphology information using open-source data. Building footprints were acquired from the Maps Static application programming interface. Building heights were extracted from an open digital surface model, i.e., the ALOS World 3D model with a resolution of 30 m (AW3D30). Thereafter, urban morphological parameters, including the sky view factor, building coverage ratio, building volume density, and frontal area density, were calculated based on the retrieved building footprints and building heights. The proposed method was applied to extract the 3D urban morphology of Hong Kong, a city with a complex urban environment and a highly mixed geographical context. The results show a usable accuracy and wide applicability for the newly proposed method.

1. Introduction

Unprecedented growth in the global population has been observed in recent decades, and 55 % of the world's population is now estimated to live in urban areas (UN DESA, 2018). The United Nations also predicts that the global population growth between 2012 and 2050 will occur mainly in cities, with close to 90 % of this increase taking place in urban areas in developing countries (UN DESA, 2015, 2018). The continual construction associated with urban sprawl has resulted in profound urban form changes, especially in less-developed countries and regions. Urban morphology includes the urban form of individual buildings, open spaces, streets, and their positions in relation to each other. Changes in urban morphology could lead to many social, economic and environmental problems, such as increasing concentrations of the population, traffic jams, housing shortages, resource shortages, biodiversity reductions, "heat island" effects, noise, and air and water pollution (Cionco & Ellefsen, 1998; Johansson, 2006; Lau, Chung, & Ren, 2019; Ng, Yuan, Chen, Ren, & Fung, 2011; Nichol, 1996; Wang et al., 2019; Wong et al., 2011; Yu, Liu, Wu, & Lin, 2009). A sustainable urban environment can help mitigate or eliminate these problems, and urban morphology information can provide fundamental data for sustainable urban development in urban planning, construction, transportation, energy and property management, environmental exposure, and so on (Suveg & Vosselman, 2004; Shearer et al., 2006; Diamantini & Zanon, 2000). Therefore, a rapid and consistent methodology for acquiring urban morphological data is paramount for developing sustainable environments for cities, especially those subject to rapid urbanization that also suffer from a lack of urban data.

However, generally applicable methods for using open-source data in cities worldwide are still deficient. Field surveys have been used to collect 3D urban morphology for years. However, although field surveys can be conducted to measure the footprints and heights of buildings, they are often labor intensive and time consuming, and only limited urban areas can be covered by conventional ground surveys. Field measurements are also prone to sampling errors, especially when volunteer-based personnel or those who are not experts are involved in the data collection (Nowak, Hirabayashi, Bodine, & Greenfield, 2014).

Satellite image-based methods for the extraction of urban morphology have been addressed by many researchers. Compared with conventional manual methods, satellite-based technologies are fast and

* Corresponding author at: Rm 505, AIT Bldg, School of Architecture, The Chinese University of Hong Kong, Shatin, New Territories, Hong Kong, China.
E-mail address: caimeng@link.cuhk.edu.hk (M. Cai).

https://doi.org/10.1016/j.scs.2019.101962
Received 29 August 2019; Received in revised form 13 November 2019; Accepted 13 November 2019
Available online 14 November 2019

Nomenclature

3D	3-Dimensional
LiDAR	Light Detection and Ranging
SAR	Synthetic Aperture Radar
InSAR	Interferometric Synthetic Aperture Radar
DSM	Digital Surface Model
OSM	OpenStreetMap
API	Application Programming Interface
GSV	Google Street View
DEM	Digital Elevation Model
BCR	Building Coverage Ratio
BVD	Building Volume Density
FAD	Frontal Area Density
SRTM	Shuttle Radar Topography Mission
ASTER GDEM	The Advanced Spaceborne Thermal Emission and Reflection Radiometer Global Digital Elevation Model
ALOS	Advanced Land Observing Satellite
AW3D30	Advanced Land Observing Satellite World 3D – 30 m
BH	Building height
nDSM	Normalized DSM
WRF	Weather Research and Forecasting
RMSE	Root Mean Square Error

economical at obtaining urban morphological information over large areas. Various remotely sensed data have been used to derive urban information, including optical images (Hao, Zhang, & Cao, 2016; Paparoditis, Cord, Jordan, & Cocquerez, 1998; Shufelt, 1999; Turker & Koc-San, 2015) and synthetic aperture radar (SAR) (Gamba, Houshmand, & Saccani, 2000; He, Jäger, Reigber, & Hellwich, 2008; Simonetto, Oriot, Garello, & Le Caillec, 2003), Light Detection and Ranging (LiDAR) (Rottensteiner & Briese, 2002; Shan & Sampath, 2017; Verma, Kumar, & Hsu, 2006; Zhou & Neumann, 2008), and interferometric SAR (InSAR) data (Burkhart et al., 1996; Gamba et al., 2000; Luckman & Grey, 2003; Thiele, Cadario, Schulz, Thonnessen, & Soergel, 2007; Dubois, Thiele, & Hinz, 2016). In addition, some research studies have extracted building information by integrating different sources of satellite images to fully exploit the advantages of different data. For example, Xu et al. (2017a) extracted building information from a high-density urban area using both high-resolution stereo and SAR data. Wegner, Ziehn, and Soergel (2010) used both optical imagery and InSAR data to detect 3D building information. Gamba and Houshmand (2002) used SAR and LiDAR data with optical imagery to detect land cover types, a DTM and the 3D shapes of buildings. Moreover, an increasing number of methods for the detection of building information are based on high-resolution digital surface models (DSMs) generated from satellite images (Davydova, Cui, & Reinartz, 2016; Lafarge, Descombes, Zerubia, & Pierrot-Deseilligny, 2010; Merciol & Lefèvre, 2015). However, the accuracy and the universality of the applicability of satellite image-based methods have been limited by the cost or accessibility of high-spatial-resolution remotely sensed data (Weidner & Förstner, 1995). Moreover, the interpretation of satellite (e.g., SAR and LiDAR) images is also complicated.

Nevertheless, recent developments in location-based services and digital map services have facilitated various applications for the extraction of urban morphological information. Several open map services, including OpenStreetMap (OSM), ArcGIS Online, Google Maps, Yahoo! Maps, and TIGER/Line Map, have been applied to extract urban information (Chiang, Knoblock, Shahabi, & Chen, 2009; Malarvizhi, Kumar, & Porchelvan, 2016; Huber & Rust, 2016; Kaiser et al., 2017). While OSM has been applied for some urban studies (Audebert, Le Saux, & Lefèvre, 2017; Lopes, Fonte, See, & Bechtel, 2017), the function and architectural details of the buildings extracted through OSM still need to be improved (Fan, Zipf, Fu, & Neis, 2014; Hecht, Kunze, & Hahmann, 2013). Google has developed a series of application programming interfaces (APIs) that allow users to extract useful urban information from Google Maps. For example, many researchers have extracted urban canopy geometries from street-view panoramas using the Google Street View (GSV) API. Openness and greenery along a street can be mapped by calculating the sky view factor (SVF) and green view index using GSV panoramas (Carrasco-Hernandez, Smedley, & Webb, 2015; Gong et al., 2018; Li, Ratti, & Seiferling, 2017; Yin & Wang, 2016; Zeng, Lu, Li, & Li, 2018). Although GSV images are free and their developed results show high accuracy, they have a well-known limitation in their spatial coverage and accessibility. Moreover, GSV images are available and applicable only for mapping the streetscapes of urban canyons in cities throughout the world and along major routes where the Google car can travel. For other cities or other urban areas where the Google car is not allowed, it is impossible to obtain any comprehensive morphological information from GSV images.

The new trend in the extraction of 3D urban morphology consists of the combination of satellite images with open map services (Haala & Anders, 1996; Over, Schilling, Neubauer, & Zipf, 2010; Suveg & Vosselman, 2004). By combining satellite images with open map services, the specific advantages of both satellite images (i.e., a high accuracy and a large information content) and maps (i.e., a relatively simple interpretation and open access availability) can be exploited. Therefore, the aims of this study are (1) to develop a method for the acquisition of 3D urban morphology information by integrating Google Maps with a freely available DSM that can be easily applied to cities worldwide; (2) to generate 3D urban morphologies and calculate urban morphological parameters in Hong Kong, a city with a complex urban form; (3) to validate the urban morphology information pertaining to various urban landscapes; and (4) to further discuss the limitations and advantages of this method, as well as its applications. The proposed method will contribute to the scholarly understanding and extraction of urban morphology in a highly efficient way using a simple workflow. This approach can be applied to cities worldwide, especially those that lack urban data. In practice, the results provide not only access to a freely open urban dataset for researchers, town planners and architects but also new insights into applications such as urban studies and urban planning related to or based on urban morphology.

2. Materials and methods

2.1. Study area and sample sites

In this study, Hong Kong — a large city with a complex urban morphology and a unique geographical context — is selected as the testbed. Hong Kong is one of the world's most compact cities, with a population of over 7.3 million in a land area of 1,100 km^2. This extremely high population density shapes the unique urban form of Hong Kong's metro area. The high-density areas of Hong Kong are almost entirely composed of densely packed high-rise buildings with podiums and deep street canyons (Li et al., 2012). As a consequence of this high density, Hong Kong is facing undesirable externalities such as thermal comfort issues, overcrowding, urban heat island effects, poor air ventilation, and high air pollution concentrations in deep street canyons. To improve the urban climate and environment, the strategic study entitled "Hong Kong 2030+: Towards a Planning Vision and Strategy Transcending 2030" (Planning Department of Hong Kong, 2016) has defined the future key strategic planning direction as "Planning for a Livable High-density City", which includes the sensitive disposition of urban blocks, building setbacks, and the creation of a breezeway/urban wind corridor, among other components.

For this study, a total of 12 rectangular areas (2 km × 2 km) with varied urban landscapes have been sampled for the extraction of 3D urban morphology information to provide a fair representation of Hong Kong's urban form, as shown in Fig. 1. Six sample sites are located in metropolitan areas (sites 5, 6, 7, 10, 11, and 12); four sites are located in the new town areas (sites 1, 4, 8, and 9); and two sites are chosen from industrial and rural areas (sites 2 and 3). The metropolitan sample areas are highly urbanized and contain a number of extremely tall skyscrapers over 200 m; the dominant building type is very tall and sharp-edged buildings (Renganathan, 2005). The sample sites located in the new town areas have more open spaces and street canyons with a relatively low height-width ratio. According to a local climate zone mapping of Hong Kong conducted by Wang, Ren, Xu, Lau, and Shi (2018), the main type of built-up structure in the Kowloon district (metropolitan area) is the compact high-rise, and the main type of built-up structure in the Yuen Long district (new town area) is sparse construction. The podium-tower structure is the most generic planning model and can be commonly found throughout Hong Kong (Ng et al., 2005).

2.2. Data source

2.2.1. Maps static API

Google Maps is an Internet open map service application and technology provided by Google that contains an urban morphology database for global cities. Google encourages the diverse usage of its products according to the Google Permissions of Using Google Maps, Google Earth and Street View (Google, 2015). Google launched the Google Maps API in June 2005 to allow developers to integrate Google Maps into their websites. The Maps Static API provided by Google Maps creates maps based on URL parameters sent through a standard HTTP request and returns the maps as an image (Google, 2018). The basic parameters that define a map include the "center coordinates", a "zoom" level and the "size" of the map image (in pixels). Optionally, by using the Maps Static API, users can employ the "style" parameter, which defines a custom style to alter the presentation of specific features (roads, parks, built-up areas, and building footprints) within the map; this parameter takes "feature" and "element" arguments, identifying the abovementioned features based on a user-defined style and a set of style operations to apply the selected features, making the map a styled map. Therefore, building footprint information can be retrieved from styled maps using the Maps Static API.

2.2.2. Digital surface model data

There are two main categories of globally available digital elevation models (DEMs): commercial DEMs and freely available DEMs. The Shuttle Radar Topography Mission (SRTM), the Advanced Spaceborne Thermal Emission and Reflection Radiometer Global DEM (ASTER GDEM), and the Advanced Land Observing Satellite (ALOS) World 3D – 30 m (AW3D30) DSM are the three global-scale DEM datasets that are currently available to the general public free of charge. All of these DEM datasets provide a moderate resolution of approx. 30 m (1 arcsec) and capture almost the entire Earth's surface. According to previous studies (Grohmann, 2018; Santillan & Makinano-Santillan, 2016), the AW3D30 DSM was found to be the most accurate DEM dataset with the lowest mean error and root mean square error (RMSE) compared to other freely available DEMs. Additionally, AW3D30 is the newest global DEM dataset currently available; it was created based on the original images from 2006 to 2011 acquired by the 5-meter mesh ALOS dataset, which is considered to be the most precise global elevation dataset at present (Tadono et al., 2014). Therefore, in this study, the AW3D30 dataset was selected for extracting building height information. The AW3D30 dataset, which was released in 2015 by the Japan Aerospace Exploration Agency, can be publicly obtained from http://www.eorc.jaxa.jp/ALOS/en/aw3d30/. The AW3D30 tiles were downloaded and saved in GeoTIFF format for further calculations using ArcMap 10.6 software.

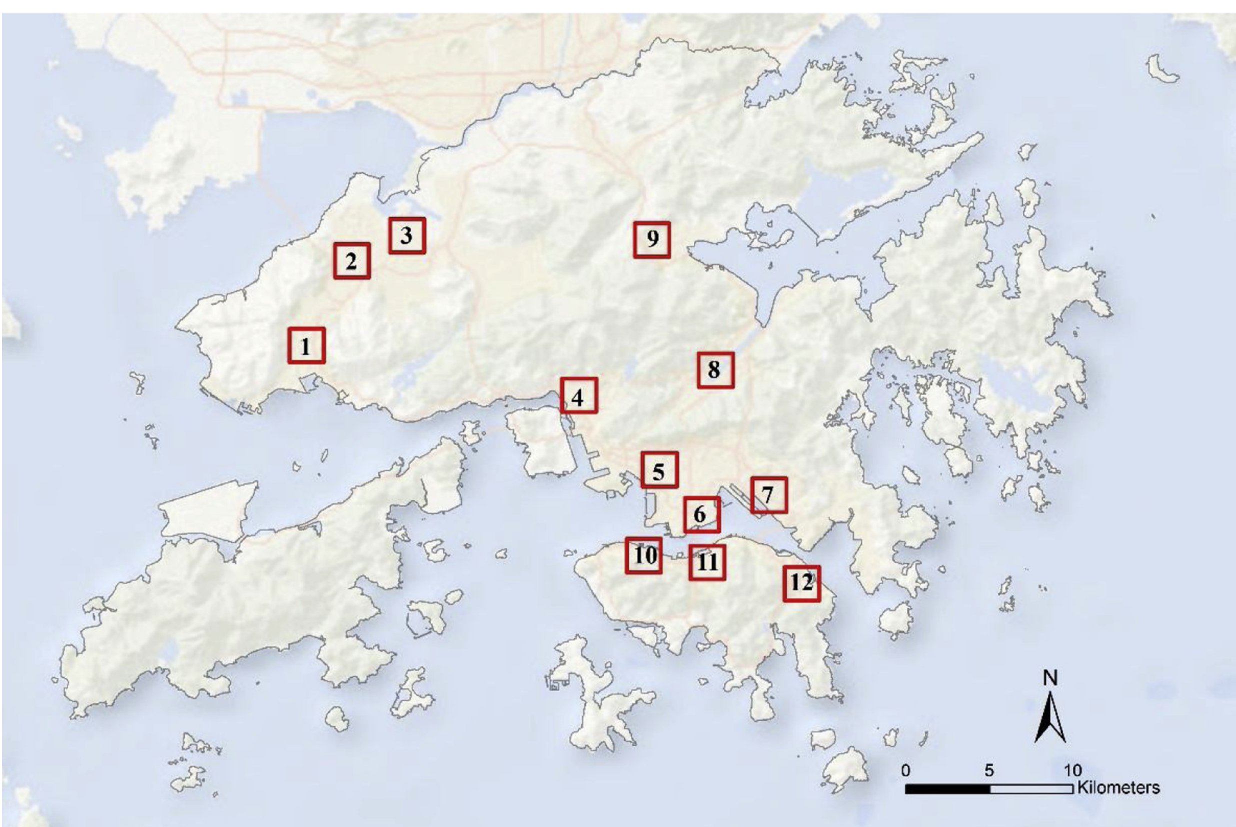

Fig. 1. The locations of the 12 sample sites (2 km × 2 km) in Hong Kong.

2.3. 3D urban morphology extraction

The process of extracting urban morphology information includes two major steps: 1) building footprint extraction and 2) building height extraction (Fig. 2). The building footprint extraction process was based on the styled maps obtained from the Maps Static API, while the building heights were generated from the AW3D30 DSM. After extracting the building heights and building footprints, the estimated urban morphology within the study area was acquired. Thereafter, urban morphological parameters, including the SVF, building coverage ratio (BCR), building volume density (BVD), and frontal area density (FAD), were calculated based on the retrieved building footprints and building heights.

2.3.1. Building footprint extraction

The presentation of standard Google Maps can be customized by applying customized styles using the Maps Static API. Therefore, styled maps can display features such as roads, parks, built-up areas, and other points of interest. The particular styles can be highlighted by defining the color or style by complementing the surrounding content on the page or even hiding features completely using the API. A Maps Static API URL must be of the following form: https://maps.googleapis.com/maps/api/staticmap?parameters.

The parameters in the URL include location, map, feature and element parameters. The location parameters determine the center coordinates of the map and the zoom level. The map parameters define the characters of the map, such as its size and format. The feature and element parameters determine the style of the map. The feature parameters indicate the presence of elements on the map, such as roads, parks, or other points of interest; for example, the syntax “feature:road” specifies the selection of roads on the map. Elements, such geometries and labels, are characteristics of features.

To display the building footprint information, styled maps within the study area were created using the Maps Static API. The location of each map was defined in the study area, and the zoom level was set to 17 to display the building footprints by setting the location parameters. The images were formatted as png32, which provides a lossless compression of the map. The features of the building footprints were selected by defining the feature parameters, and the buildings were given black outlines using the element parameters. Other features, such as roads and water, were turned off, and the background was set to white to emphasize the building footprints in each map. An example of a URL employed to retrieve a styled map has been included in the supplementary materials. The building footprints retrieved by the URLs are displayed in Fig. 3.

The maps were saved to local hard drives. The imagery was digitized in ArcScan using ArcGIS to convert the building footprints into a vector format. ArcScan provides tools to convert raster images into vector-based feature layers in a rapid and automatic way. After digitization, a spatial adjustment was performed to assign the coordinate system to the Hong Kong 1980 grid system for the retrieved vector based on actual GIS data from the planning department of Hong Kong. The details of the extracted building footprints within the study area are displayed in Figs. 4 and S1 (in the Supplementary materials).

2.3.2. Building height extraction

The building height (BH) is an important urban morphological parameter that is widely used in weather forecasting models and urban canopy models. In this study, AW3D30 DSM images were used to extract building height information. The whole processing workflow for extracting the building height consists of two stages. The first stage is the generation of an nDSM. A DSM is a representation of the Earth’s surface that contains all objects higher than the ground, e.g., trees and buildings. To extract buildings, an approximation of the bare earth (a continuous ground terrain, known as a digital elevation model, DEM) was determined first to separate the nonground objects from the ground. The difference between the original DSM and the approximated DEM is named the normalized DSM (nDSM), which contains the height information of all nonground objects (Eq. (1)).

$$nDSM = DSM - DEM \tag{1}$$

For this study, the block minimum filtering method (Wack & Wimmer, 2002) was adopted to generate the DEM by taking the minimum elevation within a certain area. Considering the resolution of the raw DSM images, the block minimum filter was applied with a grid size of 300 m. The second stage of building height extraction is to separate buildings from other objects by assigning the nDSM to each building footprint using the building information acquired from the Maps Static API. In this study, BH refers to the average building height of an individual building. The estimated building heights within the sites of the study area are displayed in Fig. 5.

2.3.3. Derivation of urban morphological parameters

The building coverage ratio (BCR) is the ratio of the building area to the total land lot size. The BCR has a strong influence on the local thermal environment (Zhan, Meng, & Xiao, 2015) and has an impact on local wind velocity ratios (Kubota, Miura, Tominaga, & Mochida, 2008; Ng et al., 2011). The results show that the higher the gross BCR is, the lower the observable wind velocity ratio will be. The BCR is calculated as follows:

$$\mathrm{BCR}=\frac{\sum_{i=1}^{N} C_i}{S_L} \tag{2}$$

where C_i is the area of building i on the plan area and S_L is the size of the plan area.

The building volume density (BVD) represents the building density over the land lot size. The BVD also influences the local thermal environment (Chen et al., 2012). The BVD is calculated as the total volume of buildings divided by the land lot size:

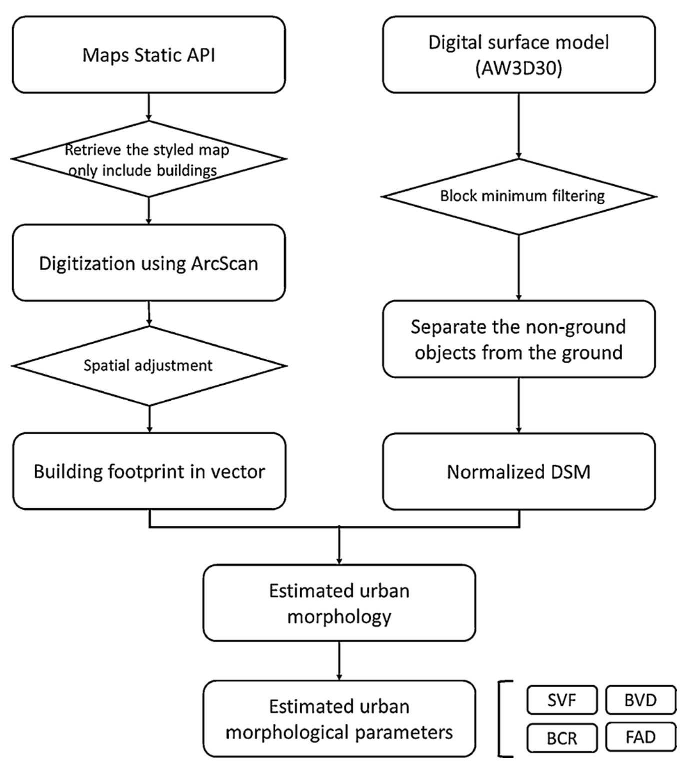

Fig. 2. A chart of the workflow for the 3D urban morphology extraction process proposed in this study.

Fig. 3. Building footprints from the Maps Static API (map center: 22.33, 114.16, zoom = 17).

$$\text{BCR}=\frac{\sum_{i=1}^{N}(C_i \times h_i)}{S_L} \tag{3}$$

where C_i is the area of building i on the land lot, h_i is the height of building i and S_L is the size of the plan area.

The sky view factor is defined as "the ratio of the amount of the sky 'seen' from a given point on a surface to that potentially available (i.e., the proportion of the sky hemisphere subtended by a horizontal surface)" (Oke, 1987, 404). The SVF can be used to quantify the ratio of the diffuse irradiance at a given point to that of an unobstructed horizontal surface. The SVF ranges between one (no influence of the adjacent terrain) and zero (no sky view and maximal influence of the adjacent terrain). The SVF is an important indicator for urban heat islands (Chen et al., 2012; Gál, Lindberg, & Unger, 2009; Scarano & Mancini, 2017). The SVF can be calculated based on DSM data by adding building heights to a DEM at a very fine scale (Dozier & Frew, 1990). In this study, the DSM newly generated from the retrieved building heights and the DEM with a 2-m resolution were used to calculate the SVF with the following expression derived from previous work (Böhner & Antonić, 2009; Scarano & Sobrino, 2015):

$$SVF=\frac{1}{2\pi}\int_0^{2\pi}[\cos\beta\cos^2\varphi+\sin\beta\cos(\phi-\alpha)(90-\varphi-\sin\varphi\cos\varphi)]d\phi \tag{4}$$

where β and α are the surface slope angle and surface aspect, respectively, calculated from the DSM, φ is the horizon angle and ϕ is the azimuth direction.

The frontal area density (FAD) refers to a building's frontal areas that face the wind over a site's area. The FAD is an important parameter for describing the surface roughness and for detecting the air paths in urban areas, which can provide a basic understanding of urban ventilation at the pedestrian level. Ng et al. (2011) conducted a study on detecting the wind environment in the Kowloon Peninsula of Hong Kong based on the FAD and found that the wind velocity ratio is more dependent on the urban morphology characteristics at the podium layer (0 − 15 m) than at the canopy layer (0 − 60 m); a 10 % increase in the FAD can result in a 2.5 % decrease in the wind velocity ratio at the podium layer. The FAD in one wind direction is calculated as:

$$FAD(\theta)=\frac{\sum_i A_F(\theta)}{S} \tag{5}$$

where $A_F(\theta)$ represents the frontal area of building i in the wind direction θ and $\boldsymbol{S}$ represents the size of the uniform grid, which is chosen as 100 m, 250 m and 500 m in this study.

2.4. Validation of the results

To assess the accuracy of the extracted urban morphology, the estimated urban morphological parameters were compared with the

Fig. 4. Extraction of building footprints for site 5, shown above as an example. For all the other sites, please see Figure S1 in the supplementary materials.

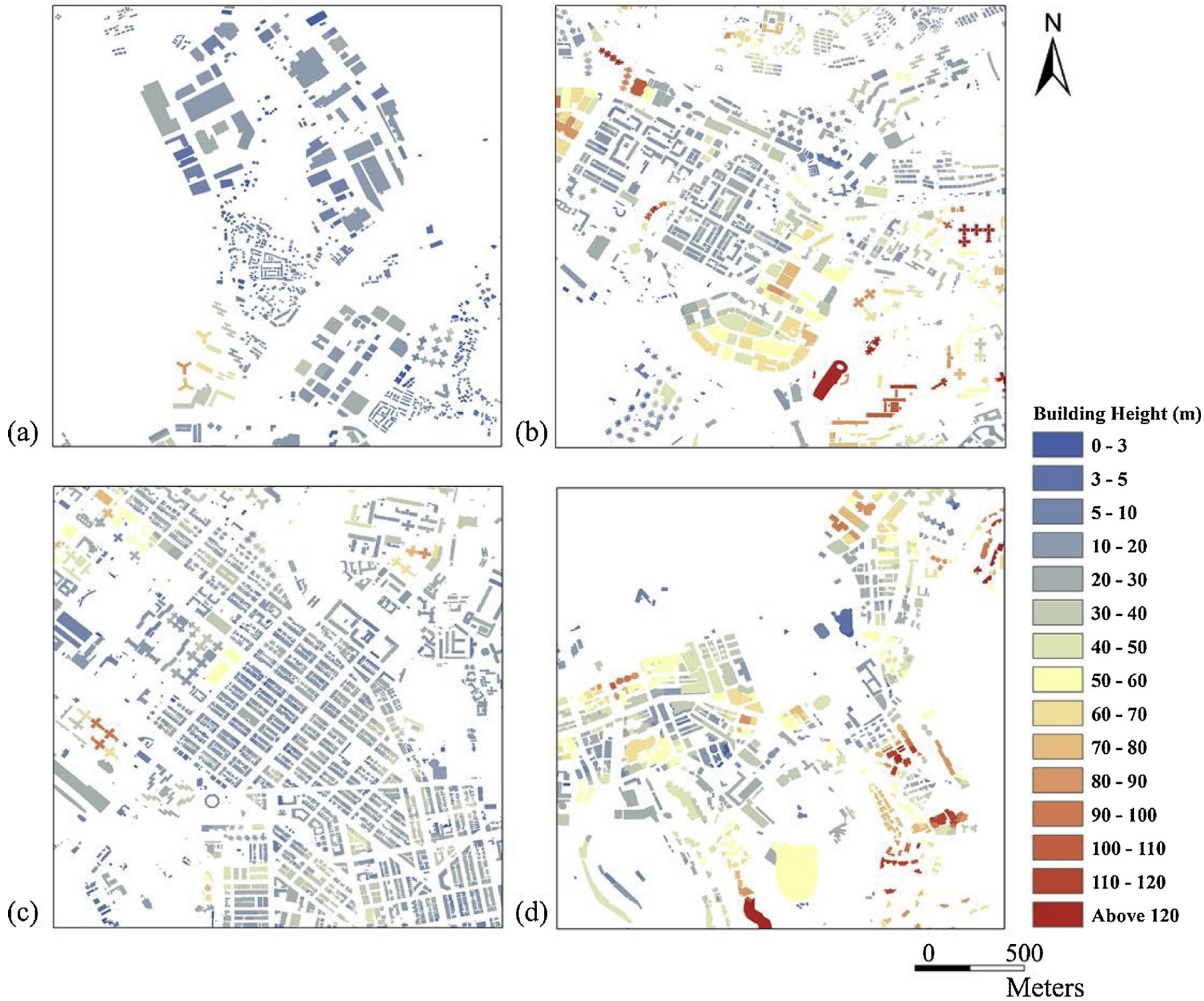

Fig. 5. The estimated building heights in (a) Site 3, (b) Site 4, (c) Site 5, and (d) Site 11.

actual parameters at resolutions of 100 m, 250 m and 500 m. First, a linear regression model was established between the estimated and actual urban morphological parameters. The R-squared value was used to assess the quality of the estimated results, where a higher R-squared value indicates a better prediction result. The calculation of R is displayed in the following equation:

$$R = \frac{n\sum_{i=1}^{n} x_i y_i - (\sum_{i=1}^{n} x_i)(\sum_{i=1}^{n} y_i)}{\sqrt{(n\sum_{i=1}^{n} x_i^2) - (\sum_{i=1}^{n} x_i)^2} \times \sqrt{(n\sum_{i=1}^{n} y_i^2) - (\sum_{i=1}^{n} y_i)^2}} \quad (6)$$

where n is the total number of observations, y is the estimated morphological parameter, and x is the actual morphological parameter. Second, the root mean square error (RMSE) was calculated to examine the errors of the predicted results. The RMSE is a quadratic scoring rule that also measures the average magnitude of the error; it is the square root of the average of the squared differences between the predicted values and the actual observations. The lower the RMSE is, the better the estimates are.

$$RMSE = \sqrt{\frac{1}{n}\sum_{i=1}^{n}(y_i - x_i)^2} \quad (7)$$

3. Results

Based on the retrieved urban morphology information, a set of urban morphological parameters was further calculated and aggregated at resolutions of 100 m, 250 m and 500 m to test the accuracy and possible applications of the results at different scales. Fig. 6 shows the actual and estimated urban morphological parameters at grid resolutions of 100 m, 250 m and 500 m.

4. Discussion

4.1. Analyzing the results of extracting building morphological parameters

4.1.1. Building coverage ratio

The validation of the results based on the 100 m grid shows good consistency between the actual and estimated BCR values with an $R^2 = 0.736$ and an RMSE of less than 9 %. As shown in the regression plot of the BCR at a 100 m grid size, a slight but systematic underestimation can be clearly observed. This underestimation not only appears at specific intervals but can be seen along almost the entire range of the data. With an increase in the grid size, the level of underestimation decreases. The relationship between the actual and estimated BCR values further increases to $R^2 = 0.824$ at a grid size of 250 m and $R^2 = 0.892$ at a grid size of 500 m. These results indicate that the estimated BCR using the method proposed herein can fulfill the requirements of input data for meteorological research and weather forecasting models, such as the Weather Research and Forecasting (WRF) model. Moreover, the estimation results at 250 m could be

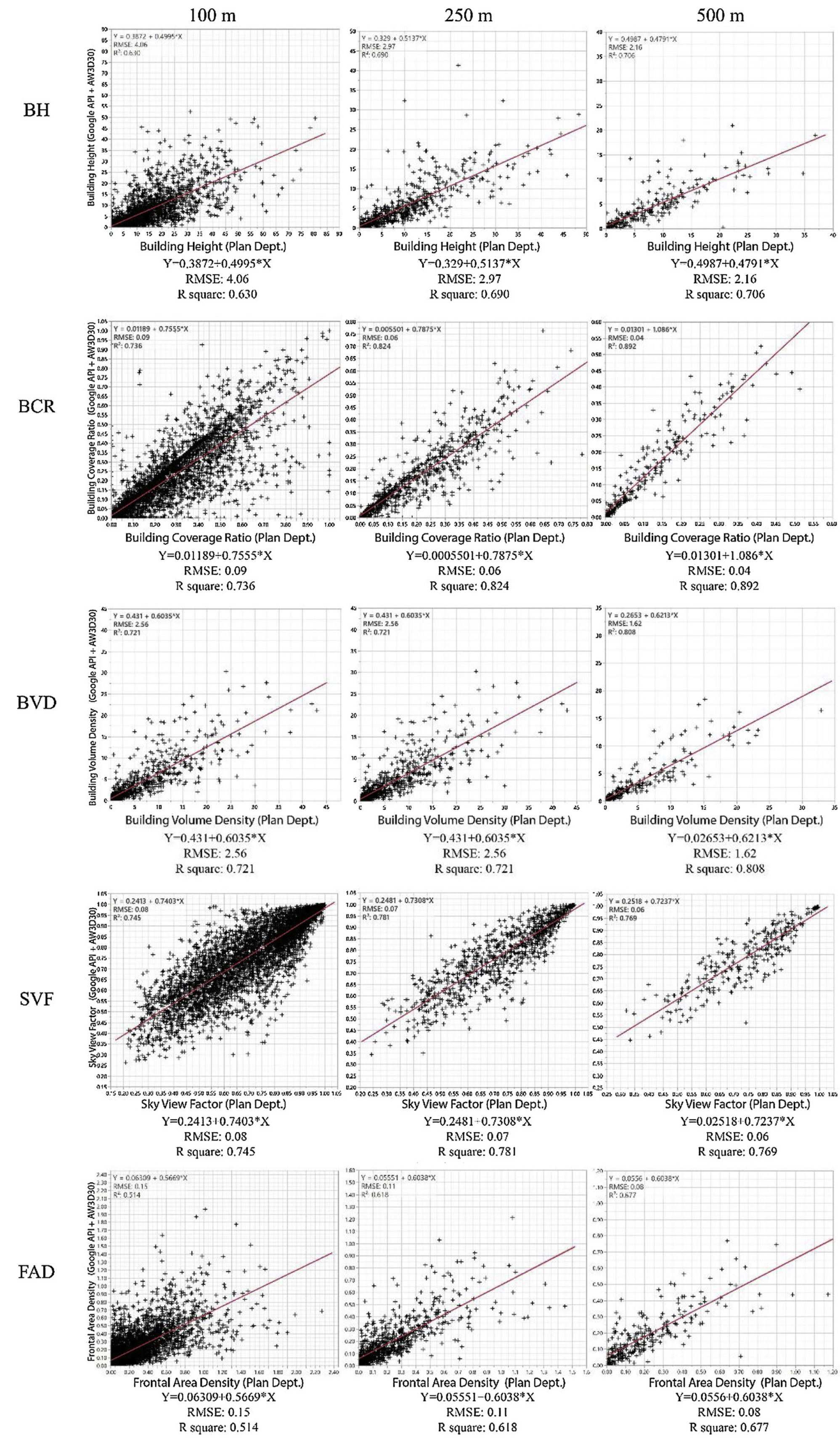

Fig. 6. The actual and estimated urban morphological parameters at grid resolutions of 100 m, 250 m and 500 m.

adopted for research at a fine spatial scale because these results already provide a reasonably accurate depiction of single urban neighborhoods and small street blocks, potentially providing a valuable input dataset for reducing the spatial uncertainties in environmental health risk assessments.

4.1.2. Building height

The estimation of the building height has a reasonable relationship with R^2 values of 0.630, 0.690, and 0.706 at grid sizes of 100 m, 250 m and 500 m, respectively. Similar to the estimation of the BCR, a general slight underestimation is observed. In contrast to the BCR estimation, however, the estimation performance of the BH does not increase considerably as the grid size increases. For example, the performance increases only slightly, by approximately 11 %, when the grid size is enlarged by a factor of five. Moreover, the regression analysis also indicates that the regression relationship between the actual and estimated BH values varies among different urban forms. As indicated in the regression plot of the BH at a grid size of 100 m, the Hung Hom site in the Kowloon Peninsula has a significant difference (the different relationship is shown as the separately plotted red regression line). Moreover, the estimation results for areas with generally low building heights are unsatisfying, which may limit the application of the proposed method in urban forms with a low-rise building environment. As indicated by these findings from the BH estimation, nonlinear fitting models are needed for further investigation and might need to be incorporated into the algorithm for improving the proposed method.

4.1.3. Building volume density

A slight overall underestimation was also observed in the estimation of the BVD at all grid sizes. This might be a result of the observed underestimation in both the BCR and the BH. However, there are no particular patterns among the different quantiles of the BVD. The outliers are mostly randomly distributed along both sides of the regression line. Similar to the BCR estimation results, there is consistency between the actual and estimated values since the R^2 values increase from 0.599 to 0.808 as the grid size increases. The proposed method provides a usable estimation of the BVD at a 500 m spatial resolution, which is potentially applicable as an input to regional meteorological and weather forecasting models. However, the overall underestimation mentioned above will need to be calibrated based on site survey data.

4.1.4. Sky view factor

For the relationship between the SVF calculated based on actual building data and that based on estimated building data, the R^2 ranges from 0.745 to 0.781 for the three different grid sizes. Similar to the BH, the estimation performance of the SVF does not increase considerably as the grid size increases. The overall estimation performance of the SVF remains stable across different grid sizes and is therefore not sensitive to the resolution. No obvious underestimation or overestimation was identified. The above findings indicate that the building data generated by using the Google Maps API and the AW3D30 dataset provide a reasonably good estimation of the SVF (Fig. 7). Considering that the results remain stable at varying spatial resolutions (ranging from 100 m to 500 m), the SVF estimation results are applicable to the investigation of city-scale outdoor thermal comfort; the estimated SVF could also be used as a reference for the spatial investigation of city-scale urban climate and city energy exchanges.

4.1.5. Frontal area density

Similar to the BVD, a slight overall underestimation was observed in the estimation of the FAD at all different grid sizes, which might be due to the observed underestimation in both the BCR and the BH. However, there are no particular patterns among the different quantiles of the FAD. The data points are mostly randomly distributed along both sides

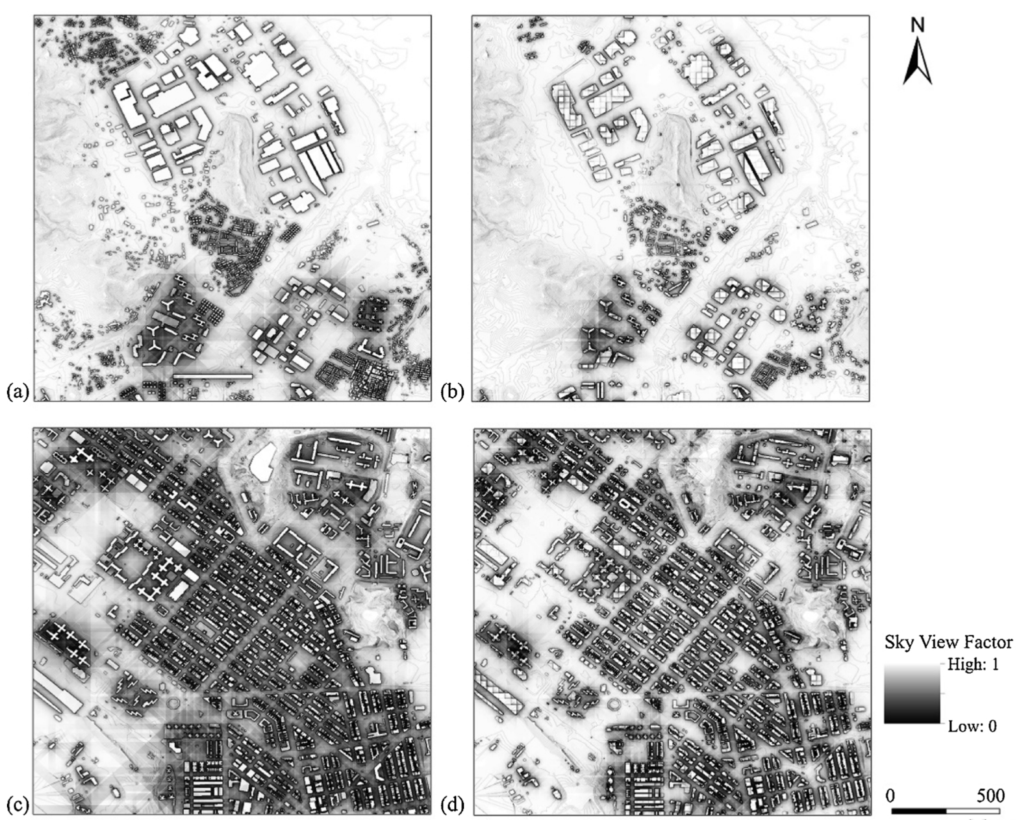

Fig. 7. (a) The actual sky view factor of Site 3. (b) The estimated sky view factor of Site 3. (c) The actual sky view factor of Site 5. (d) The estimated sky view factor of Site 5.

of the regression line. Different from the BH estimation results, the regression analysis of the estimated FAD indicates that the regression relationship between the actual and estimated BH values does not vary among different urban forms. Moreover, the estimation performance of the FAD slightly increases as the grid size increases. The R^2 values reach 0.514 and 0.618 at grid sizes of 100 m and 250 m, respectively, and a usable estimation performance of $R^2 = 0.677$ is achieved at a grid size of 500 m. These validation results indicate that the FAD estimation results acquired at a spatial resolution of 500 m by using the method proposed in the present study have the potential to be further calibrated with a site survey and subsequently adopted as input data for meteorological research and weather forecasting models, such as the WRF model. By investigating the geolocation of the outliers in the regression, it can be found that a low actual FAD in reality but a high estimated FAD in the extracted building dataset is due to an overestimation corresponding to the low-rise, sparsely built village clusters on the hillslope. To resolve this issue, the method of handling the AW3D30 dataset should be fine-tuned to correct for the estimated building heights of low-rise buildings on slopes or at relatively high elevations. A high actual FAD in reality corresponding to a low estimated FAD in the extracted building dataset is also observed, which is due to the underestimation caused by unidentified skyscraper towers atop the large building podiums in the footprint data extracted using the Google Maps API. These under/overestimations are not considered to be critical issues since the above situations are due to unique urban morphological characteristics, which do not occur frequently in most cities.

4.2. Limitations and future research

As shown in the validation of these results, although the newly developed 3D urban morphology extraction method performs reasonably well in estimating most urban morphological parameters in the majority of urban forms, slight overestimations or underestimations have been observed in the test results when applying this method in Hong Kong. By identifying the geolocations of the overestimated or underestimated areas, it has been found that many of these cases are due to the highly complex urban form of Hong Kong, which should not be as critical an issue in other cities throughout the world. More specifically, the elevation information within the AW3D30 dataset over Hong Kong tends to have a lower accuracy than the information over other cities, as it is more challenging to extract building heights from the extremely high-density and unique urban physical environment of Hong Kong (Xu et al., 2017b). All the above findings indicate that future research should focus on fine-tuning the method for handling the AW3D30 dataset to further improve the estimation of the building heights in some particular scenarios (i.e., involving low-rise buildings on sloped land or at relatively high elevations or involving skyscraper towers combined with large building podiums). Future research should also focus on testing the proposed method in other cities with varying urban morphological characteristics.

To further improve the robustness of the results in different urban scenarios all over the world, we would like to recommend that the potential users of this method conduct on-site building surveys in their own cities (or acquire building survey data from local authorities) based on a partial sampling scheme. These building survey data could be used as the ground truth for calibrating and fine-tuning the results for their particular urban forms.

Roofs are another important component of urban morphology in an urban environment. The geometry of a roof can be detected using the Maps Static API. However, variations in the roof height cannot be fully represented due to the coarse spatial resolution of the AW3D30 dataset. Thus, this study focused only on the footprints and heights of buildings.

5. Conclusions

This study developed an easy and highly efficient method for extracting 3D urban morphology information by using open-source data. Our newly developed method provides researchers with a possible way to collect 3D urban and building morphology information since all raw data are freely available and accessible to the public. The developed method consists of a two-step procedure: building footprints are extracted from styled maps using the Maps Static API, and building heights are extracted from open-source DSM data, i.e., the AW3D30 dataset. The proposed method was applied in Hong Kong, a city with a varying and complex urban morphology. The 3D urban morphology in Hong Kong was extracted using the developed approach, and the urban morphological parameters, including the building height, building coverage ratio, building volume density, sky view factor and frontal area density, were calculated. As the proposed approach is generic and uses open-source data, given the reliability of the results, this study demonstrates that the developed method could be adopted and applied to any other city or region on Earth. The urban morphological parameters estimated based on the newly compiled 3D urban morphology data were validated by a comparison with the actual parameters in different urban landscapes at various resolutions of 100 m, 250 m and 500 m to explore the potential usage of the developed methodology. The results show a reasonably good and useable accuracy and a wide applicability of the newly proposed method. In particular, a higher accuracy was identified in areas with a less complex urban form, and the accuracy increased with the spatial resolution of the urban morphological parameters. The high accuracy of the urban morphological parameters extracted based on the grid with a 500 m spatial resolution indicates that the 3D urban morphological information detected using the proposed method is readily applicable to serve as input data for mesoscale climate and environment modeling simulations, such as WRF simulations. The presented method and the retrieved variables can also be used as environmental variables in environmental exposure investigations, public health risk assessments, and urban carbon emissions mapping. Therefore, this 3D urban morphology extraction method can contribute to sustainable urban development in general and practical applications in the implementation of town planning exercises and urban development decision-making.

Declaration of Competing Interest

None.

Acknowledgments

This research is supported by the General Research Fund (GRF Project Number: 14611015, 14643816) from the Research Grants Council (RGC) of Hong Kong. Part of the research was developed during the Young Scientists Summer Program at the International Institute for Applied Systems Analysis, Laxenburg (Austria) with financial support from the Ecosystems Services and Management program. The authors appreciate reviewers for their insightful comments and constructive suggestions on our research work. The authors also want to thank editors for their patient and meticulous work for our manuscript.

Appendix A. Supplementary data

Supplementary material related to this article can be found, in the online version, at doi:https://doi.org/10.1016/j.scs.2019.101962.

References

Audebert, N., Le Saux, B., & Lefèvre, S. (2017). Joint learning from earth observation and openstreetmap data to get faster better semantic maps. *Paper Presented at the EARTHVISION 2017 IEEE/ISPRS CVPR Workshop. Large Scale Computer Vision for Remote Sensing Imagery*.

Böhner, J., & Antonić, O. (2009). Land-surface parameters specific to topo-climatology. *Developments in Soil Science, 33*, 195–226. https://doi.org/10.1016/S0166-2481(08)00008-1.

Burkhart, G., Bergen, Z., Carande, R., Hensley, W., Bickel, D., & Fellerhoff, J. (1996). Elevation correction and building extraction from interferometric SAR imagery. *Paper Presented at the Geoscience and Remote Sensing Symposium, 1996. IGARSS'96.'Remote Sensing for a Sustainable Future', International*. https://doi.org/10.1109/IGARSS.1996.516434.

Carrasco-Hernandez, R., Smedley, A. R., & Webb, A. R. (2015). Using urban canyon geometries obtained from Google Street View for atmospheric studies: Potential applications in the calculation of street level total shortwave irradiances. *Energy and Buildings, 86*, 340–348. https://doi.org/10.1016/j.enbuild.2014.10.001.

Chen, L., Ng, E., An, X., Ren, C., Lee, M., Wang, U., ... He, Z. (2012). Sky view factor analysis of street canyons and its implications for daytime intra-urban air temperature differentials in high-rise, high-density urban areas of Hong Kong: A GIS-based simulation approach. *International Journal of Climatology, 32*(1), 121–136. https://doi.org/10.1002/joc.2243.

Chiang, Y.-Y., Knoblock, C. A., Shahabi, C., & Chen, C.-C. (2009). Automatic and accurate extraction of road intersections from raster maps. *GeoInformatica, 13*(2), 121–157. https://doi.org/10.1007/s10707-008-0046-3.

Cionco, R. M., & Ellefsen, R. (1998). High resolution urban morphology data for urban wind flow modeling. *Atmospheric Environment, 32*(1), 7–17. https://doi.org/10.1016/S1352-2310(97)00274-4.

Davydova, K., Cui, S., & Reinartz, P. (2016). *Building footprint extraction from digital surface models using neural networks.* October*Image and signal processing for remote sensing XXII, Vol. 10004*, International Society for Optics and Photonics100040J. https://doi.org/10.5194/isprs-archives-XLII-1-W1-481-2017.

Diamantini, C., & Zanon, B. (2000). Planning the urban sustainable development the case of the plan for the province of Trento, Italy. *Environmental Impact Assessment Review, 20*(3), 299–310. https://doi.org/10.1016/S0195-9255(00)00042-1.

Dozier, J., & Frew, J. (1990). Rapid calculation of terrain parameters for radiation modeling from digital elevation data. *IEEE Transactions on Geoscience and Remote Sensing, 28*(5), 963–969. https://doi.org/10.1109/36.58986.

Dubois, C., Thiele, A., & Hinz, S. (2016). Building detection and building parameter retrieval in InSAR phase images. *ISPRS Journal of Photogrammetry and Remote Sensing, 114*, 228–241. https://doi.org/10.1016/j.isprsjprs.2016.02.009.

Fan, H., Zipf, A., Fu, Q., & Neis, P. (2014). Quality assessment for building footprints data on OpenStreetMap. *International Journal of Geographical Information Science, 28*(4), 700–719. https://doi.org/10.1080/13658816.2013.867495.

Gál, T., Lindberg, F., & Unger, J. (2009). Computing continuous sky view factors using 3D urban raster and vector databases: Comparison and application to urban climate. *Theoretical and applied climatology, 95*(1-2), 111–123. https://doi.org/10.1007/s00704-007-0362-9.

Gamba, P., & Houshmand, B. (2002). Joint analysis of SAR, LIDAR and aerial imagery for simultaneous extraction of land cover, DTM and 3D shape of buildings. *International Journal of Remote Sensing, 23*(20), 4439–4450. https://doi.org/10.1080/01431160110114952.

Gamba, P., Houshmand, B., & Saccani, M. (2000). Detection and extraction of buildings from interferometric SAR data. *IEEE Transactions on Geoscience and Remote Sensing, 38*(1), 611–617. https://doi.org/10.1109/36.823956.

Gong, F.-Y., Zeng, Z.-C., Zhang, F., Li, X., Ng, E., & Norford, L. K. (2018). Mapping sky, tree, and building view factors of street canyons in a high-density urban environment. *Building and Environment, 134*, 155–167. https://doi.org/10.1016/j.buildenv.2018.02.042.

Google (2015). *Permissions.* Retrieved fromhttps://www.google.com/permissions/geoguidelines/.

Google (2018). *Maps static API.* Retrieved fromhttps://developers.google.com/maps/documentation/maps-static/dev-guide.

Grohmann, C. H. (2018). Evaluation of TanDEM-X DEMs on selected Brazilian sites: Comparison with SRTM, ASTER GDEM and ALOS AW3D30. *Remote Sensing of Environment, 212*, 121–133. https://doi.org/10.1016/j.rse.2018.04.043.

Haala, N., & Anders, K.-H. (1996). Fusion of 2D-GIS and image data for 3D building reconstruction. *International Archives of Photogrammetry and Remote Sensing, 31*, 285–290.

Hao, L., Zhang, Y., & Cao, Z. (2016). Building extraction from stereo aerial images based on multi-layer line grouping with height constraint. July *2016 IEEE International Geoscience and Remote Sensing Symposium (IGARSS)* (pp. 445–448). . https://doi.org/10.1109/IGARSS.2016.7729110.

He, W., Jäger, M., Reigber, A., & Hellwich, O. (2008). Building extraction from polarimetric SAR data using mean shift and conditional random fields. In: *Paper Presented at the Proc. 7th Eur. Conf. Synth. Aperture Radar (EUSAR)*.

Hecht, R., Kunze, C., & Hahmann, S. (2013). Measuring completeness of building footprints in OpenStreetMap over space and time. *ISPRS International Journal of Geo-Information, 2*(4), 1066–1091. https://doi.org/10.3390/ijgi2041066.

Huber, S., & Rust, C. (2016). Calculate travel time and distance with OpenStreetMap data using the Open Source Routing Machine (OSRM). *The Stata Journal, 16*(2), 416–423.

Johansson, E. (2006). Influence of urban geometry on outdoor thermal comfort in a hot dry climate: A study in Fez, Morocco. *Building and Environment, 41*(10), 1326–1338. https://doi.org/10.1016/j.buildenv.2005.05.022.

Kaiser, P., Wegner, J. D., Lucchi, A., Jaggi, M., Hofmann, T., & Schindler, K. (2017). Learning aerial image segmentation from online maps. *IEEE Transactions on Geoscience and Remote Sensing, 55*(11), 6054–6068. https://doi.org/10.1109/TGRS.2017.2719738.

Kubota, T., Miura, M., Tominaga, Y., & Mochida, A. (2008). Wind tunnel tests on the relationship between building density and pedestrian-level wind velocity: Development of guidelines for realizing acceptable wind environment in residential neighborhoods. *Building and Environment, 43*(10), 1699–1708. https://doi.org/10.1016/j.buildenv.2007.10.015.

Lafarge, F., Descombes, X., Zerubia, J., & Pierrot-Deseilligny, M. (2010). Structural approach for building reconstruction from a single DSM. *IEEE Transactions on Pattern Analysis and Machine Intelligence, 32*(1), 135–147. https://doi.org/10.1109/TPAMI.2008.281.

Lau, K. K.-L., Chung, S. C., & Ren, C. (2019). Outdoor thermal comfort in different urban settings of sub-tropical high-density cities: An approach of adopting local climate zone (LCZ) classification. *Building and Environment, 154*, 227–238. https://doi.org/10.1016/j.buildenv.2019.03.005.

Li, T. T., Gao, Y. L., Wei, Z. H., Wang, J., Guo, Y. F., Liu, F., ... Cheng, Y. L. (2012). Assessing heat-related mortality risks in Beijing, China. *Biomedical and Environmental Sciences, 25*(4), 458–464. https://doi.org/10.3967/0895-3988.2012.04.011.

Li, X., Ratti, C., & Seiferling, I. (2017). Mapping urban landscapes along streets using google street view. *Paper Presented at the International Cartographic Conference*.

Lopes, P., Fonte, C., See, L., & Bechtel, B. (2017). Using OpenStreetMap data to assist in the creation of LCZ maps. *Paper Presented at the Urban Remote Sensing Event (JURSE), 2017 Joint*. https://doi.org/10.1109/JURSE.2017.7924630.

Luckman, A., & Grey, W. (2003). Urban building height variance from multibaseline ERS coherence. *IEEE Transactions on Geoscience and Remote Sensing, 41*(9), 2022–2025. https://doi.org/10.1109/TGRS.2003.815236.

Malarvizhi, K., Kumar, S. V., & Porchelvan, P. (2016). Use of high resolution google earth satellite imagery in landuse map preparation for urban related applications. *Procedia Technology, 24*, 1835–1842. https://doi.org/10.1016/j.protcy.2016.05.231.

Merciol, F., & Lefèvre, S. (2015). Fast building extraction by multiscale analysis of digital surface models. July *2015 IEEE International Geoscience and Remote Sensing Symposium (IGARSS)* (pp. 553–556). . https://doi.org/10.1109/IGARSS.2015.7325823.

Ng, E., Tam, I., Ng, A., Givoni, B., Katzschner, L., Kwok, K., ... Cheng, V. (2005). *Feasibility study for establishment of air ventilation assessment system–final report*Hong Kong: Department of Architecture, Chinese University of Hong Kong16.

Ng, E., Yuan, C., Chen, L., Ren, C., & Fung, J. C. (2011). Improving the wind environment in high-density cities by understanding urban morphology and surface roughness: A study in Hong Kong. *Landscape and Urban Planning, 101*(1), 59–74. https://doi.org/10.1016/j.landurbplan.2011.01.004.

Nichol, J. E. (1996). High-resolution surface temperature patterns related to urban morphology in a tropical city: A satellite-based study. *Journal of Applied Meteorology, 35*(1), 135–146.

Nowak, D. J., Hirabayashi, S., Bodine, A., & Greenfield, E. (2014). Tree and forest effects on air quality and human health in the United States. *Environmental Pollution, 193*, 119–129. https://doi.org/10.1016/j.envpol.2014.05.028.

Oke, T. R. (1987). *Boundary layer climates.* Routledge.

Over, M., Schilling, A., Neubauer, S., & Zipf, A. (2010). Generating web-based 3D City Models from OpenStreetMap: The current situation in Germany. *Computers, Environment and Urban Systems, 34*(6), 496–507. https://doi.org/10.1016/j.compenvurbsys.2010.05.001.

Paparoditis, N., Cord, M., Jordan, M., & Cocquerez, J.-P. (1998). Building detection and reconstruction from mid-and high-resolution aerial imagery. *Computer Vision and Image Understanding, 72*(2), 122–142. https://doi.org/10.1006/cviu.1998.0722.

Planning Department of Hong Kong (2016). *Hong Kong 2030+ planning and urban design for a liveable high-density city.* Retrieved fromhttp://www.hk2030plus.hk/document/Planning%20and%20Urban%20Design%20for%20a%20Liveable%20High-Density%20City_Eng.pdf.

Renganathan, G. J. H. T. O. (2005). *Urban design factors influencing outdoor temperature in high-risehigh-density residential developments in the coastal zone of Hong Kong.* HKU Theses Online (HKUTO).

Rottensteiner, F., & Briese, C. (2002). A new method for building extraction in urban areas from high-resolution LIDAR data. *International Archives of Photogrammetry Remote Sensing and Spatial Information Sciences, 34*(3/A), 295–301.

Santillan, J. R., & Makinano-Santillan, M. (2016). Vertical accuracy assessment of 30-M resolution Alos, Aster, And Srtm global Dems over Northeastern Mindanao, Philippines. *International Archives of the Photogrammetry, Remote Sensing & Spatial Information Sciences, 41*, 149–156. https://doi.org/10.5194/isprsarchives-XLI-B4-149-2016.

Scarano, M., & Mancini, F. (2017). Assessing the relationship between sky view factor and land surface temperature to the spatial resolution. *International Journal of Remote Sensing, 38*(23), 6910–6929. https://doi.org/10.1080/01431161.2017.1368099.

Scarano, M., & Sobrino, J. (2015). On the relationship between the sky view factor and the land surface temperature derived by Landsat-8 images in Bari, Italy. *International Journal of Remote Sensing, 36*(19–20), 4820–4835. https://doi.org/10.1080/01431161.2015.1070325.

Shan, J., & Sampath, A. (2017). *Building extraction from LiDAR point clouds based on clustering techniques. Topographic laser ranging and scanning.* CRC Press421–444.

Shearer, A. W., Mouat, D. A., Bassett, S. D., Binford, M. W., Johnson, C. W., & Saarinen, J. A. (2006). Examining development-related uncertainties for environmental management: Strategic planning scenarios in Southern California. *Landscape and Urban Planning, 77*(4), 359–381. https://doi.org/10.1016/j.landurbplan.2005.04.005.

Shufelt, J. A. (1999). Performance evaluation and analysis of monocular building extraction from aerial imagery. *IEEE Transactions on Pattern Analysis and Machine Intelligence, 21*(4), 311–326. https://doi.org/10.1109/34.761262.

Simonetto, E., Oriot, H., Garello, R., & Le Caillec, J. (2003). Radargrammetric processing for 3-D building extraction from high-resolution airborne SAR data. *Paper Presented at the INTERNATIONAL GEOSCIENCE AND REMOTE SENSING SYMPOSIUM*. https://doi.org/10.1109/IGARSS.2003.1294320.

Suveg, I., & Vosselman, G. (2004). Reconstruction of 3D building models from aerial images and maps. *ISPRS Journal of Photogrammetry and Remote Sensing, 58*(3), 202–224. https://doi.org/10.1016/j.isprsjprs.2003.09.006.

Tadono, T., Ishida, H., Oda, F., Naito, S., Minakawa, K., & Iwamoto, H. (2014). Precise global DEM generation by ALOS PRISM. *ISPRS Annals of the Photogrammetry, Remote Sensing and Spatial Information Sciences, 2*(4), 71. https://doi.org/10.5194/

isprsannals-II-4-71-2014.

Thiele, A., Cadario, E., Schulz, K., Thonnessen, U., & Soergel, U. (2007). Building recognition from multi-aspect high-resolution InSAR data in urban areas. *IEEE Transactions on Geoscience and Remote Sensing, 45*(11), 3583–3593. https://doi.org/10.1109/TGRS.2007.898440.

Turker, M., & Koc-San, D. (2015). Building extraction from high-resolution optical spaceborne images using the integration of support vector machine (SVM) classification, Hough transformation and perceptual grouping. *International Journal of Applied Earth Observation and Geoinformation, 34*, 58–69. https://doi.org/10.1016/j.jag.2014.06.016.

UN DESA (2015). *World population projected to reach 9.7 billion by 2050. United Nations homepage New York*.

UN DESA (2018). *World urbanisation prospects, 2018 revision.* Retrieved from New York.

Verma, V., Kumar, R., & Hsu, S. (2006). 3D building detection and modeling from aerial LIDAR data. *Paper Presented at the Computer Vision and Pattern Recognition, 2006 IEEE Computer Society Conference on*. https://doi.org/10.1109/CVPR.2006.12.

Wack, R., & Wimmer, A. (2002). Digital terrain models from airborne laserscanner data-a grid based approach. *International Archives of Photogrammetry Remote Sensing and Spatial Information Sciences, 34*(3/B), 293–296.

Wang, R., Ren, C., Xu, Y., Lau, K. K.-L., & Shi, Y. (2018). Mapping the local climate zones of urban areas by GIS-based and WUDAPT methods: A case study of Hong Kong. *Urban Climate, 24*, 567–576. https://doi.org/10.1016/j.uclim.2017.10.001.

Wang, R., Cai, M., Ren, C., Bechtel, B., Xu, Y., & Ng, E. (2019). Detecting multi-temporal land cover change and land surface temperature in Pearl River delta by adopting local climate zone. *Urban Climate, 28*, 100455. https://doi.org/10.1016/j.uclim.2019.100455.

Wegner, J. D., Ziehn, J. R., & Soergel, U. (2010). Building detection and height estimation from high-resolution InSAR and optical data. *Paper Presented at the Geoscience and Remote Sensing Symposium (IGARSS), 2010 IEEE International*. https://doi.org/10.1109/IGARSS.2010.5653386.

Weidner, U., & Förstner, W. (1995). Towards automatic building extraction from high-resolution digital elevation models. *ISPRS journal of Photogrammetry and Remote Sensing, 50*(4), 38–49. https://doi.org/10.1016/0924-2716(95)98236-S.

Wong, N. H., Jusuf, S. K., Syafii, N. I., Chen, Y., Hajadi, N., Sathyanarayanan, H., ... Manickavasagam, Y. V. (2011). Evaluation of the impact of the surrounding urban morphology on building energy consumption. *Solar Energy, 85*(1), 57–71. https://doi.org/10.1016/j.solener.2010.11.002.

Xu, Y., Ren, C., Ma, P., Ho, J., Wang, W., Lau, K. K.-L., ... Ng, E. (2017a). Urban morphology detection and computation for urban climate research. *Landscape and Urban Planning, 167*, 212–224. https://doi.org/10.1016/j.landurbplan.2017.06.018.

Xu, Y., Ren, C., Ma, P., Ho, J., Wang, W., Lau, K. K.-L., ... Ng, E. (2017b). Urban morphology detection and computation for urban climate research. *Landscape and Urban Planning, 167*(Supplement C), 212–224. https://doi.org/10.1016/j.landurbplan.2017.06.018.

Yin, L., & Wang, Z. (2016). Measuring visual enclosure for street walkability: Using machine learning algorithms and Google Street View imagery. *Applied Geography, 76*, 147–153. https://doi.org/10.1016/j.apgeog.2016.09.024.

Yu, B., Liu, H., Wu, J., & Lin, W.-M. (2009). Investigating impacts of urban morphology on spatio-temporal variations of solar radiation with airborne LIDAR data and a solar flux model: A case study of downtown Houston. *International Journal of Remote Sensing, 30*(17), 4359–4385. https://doi.org/10.1080/01431160802555846.

Zeng, L., Lu, J., Li, W., & Li, Y. (2018). A fast approach for large-scale sky view factor estimation using street view images. *Building and Environment, 135*, 74–84. https://doi.org/10.1016/j.buildenv.2018.03.009.

Zhan, Q., Meng, F., & Xiao, Y. (2015). Exploring the relationships of between land surface temperature, ground coverage ratio and building volume density in an urbanized environment. *The International Archives of Photogrammetry, Remote Sensing and Spatial Information Sciences, 40*(7), 255. https://doi.org/10.5194/isprsarchives-XL-7-W3-255-2015.

Zhou, Q.-Y., & Neumann, U. (2008). Fast and extensible building modeling from airborne LiDAR data. *Paper Presented at the Proceedings of the 16th ACM SIGSPATIAL International Conference on Advances in Geographic Information Systems*. https://doi.org/10.1145/1463434.1463444.